International Journal for Housing Science and Its Applications
Publish August 10, 2025. Volume 46, Issue 4 Pages 8268-8283

https://doi.org/10.70517/ijhsa464707

# Building elevator bearing diagnosis based on feature dimensionality reduction and parameter optimization

**Qiang Li[1], Rundong Zhou[1], Xinyu Zhai[1] and Qing Lv[1,*]**
[1] Vocational and Technical College, Hebei Normal University, Shijiazhuang, Hebei, 050024, China
Corresponding authors: (e-mail: lvqing@hebtu.edu.cn).

**Abstract** The elevator is a vital apparatus in everyday life, and precise fault identification is critical for guaranteeing its safe operation. This paper offers an elevator bearing fault diagnosis approach utilizing MHO-BPNet, as current methods frequently exhibit low accuracy rates. The main aspects of this method are: first, redundant and noisy features are removed using Mean Influence Value (MIV) feature dimensionality reduction method. Second, the Hippopotamus Optimization (HO) algorithm is introduced to optimize the initial weights and thresholds of the Backpropagation Neural Networks (BPNNs) in order to avoid local optimal solutions and gradient vanishing problems. Finally, the MHO-BPNet model is experimentally verified with two datasets to achieve more than 96.5% accuracy in both cases and accurately identify the fault states of the elevator.

**Index Terms** bearing, elevator, mean impact value, hippopotamus optimization algorithm, backpropagation neural network, fault diagnosis

## I. Introduction

As modern high-rise buildings gain popularity, the elevator, an essential component of these structures, is extensively scrutinized for its safety and reliability [1]. In the event of elevator failure, rolling bearings serve as critical components of the elevator drive system, and their operational status directly influences the stability of the entire system; if not detected promptly, this may result in severe safety incidents [2]. Consequently, developing effective fault diagnosis methods for elevator bearings is crucial to assure the equipment's steady operation [3].

Conventional fault diagnosis techniques depend on empirical assessment or manual signal feature extraction, resulting in low diagnostic efficiency, high subjectivity, and inadequate generalization capability [4]. In recent years, the advancement of artificial intelligence and intelligent perception technology has rendered machine learning (ML) a focal point of research in fault diagnosis, ML enabling the automatic extraction of features and the establishment of fault pattern mapping relationships from extensive data, thereby significantly enhancing diagnostic accuracy and efficiency. For example, Support Vector Machines (SVM) [5] and Multilayer Perceptron (MLP) [6] are widely used in bearing defect detection activities. Sinitsin V. et al [7]. proposed a hybrid MLP model that simultaneously handles different types of data, which not only locates the position of bearing faults but also achieves a high accuracy rate, but the method is useful for bearings of tracking actuators which operate in unsteady motion. Yanqiu Wu. et al [8]. input the extracted feature vectors into a particle swarm optimized SVM classifier and achieved more than 90% accuracy under constant speed conditions only. Kumar Rajeev et al [9]. proposed Automated fault investigation scheme (AFI) method and optimized SVM by genetic algorithm, this AFI method provides a new idea for fault diagnosis. In contrast to the aforementioned models, Backpropagation Neural Networks (BPNNs) can extract deep features incrementally through their multilayer architecture, making them more adept at addressing complex nonlinear relationships in bearing vibration signals. Additionally, the gradient descent optimization mechanism of BPNNs preserves a high level of generalization capability. The conventional BPNN is susceptible to local optima and exhibits significant sensitivity to input features; thus, it is essential to integrate an optimization method to enhance its performance.

Moreover, the extraction of feature parameters is a crucial aspect of fault diagnosis, and numerous researchers have employed various approaches to extract the feature parameters of bearings. Cheng Yang, Wang Haiming, and Li Zhen et al [10]. [11], [12] based on the combination of multi-scale arrangement entropy and other algorithmic approaches, overcame the shortcomings of the fixed MPE parameters and improved the fault recognition accuracy. Other scholars, Guo Huijia et al [13]. proposed a flexible way of feature extraction parameters, combining the time-domain joint with a hybrid deep learning model to improve the diagnostic accuracy under variable rotational speeds, loads, and strong noise disturbances. Li Yun et al [14]. combined the autocorrelation function and the improved multi-point optimal minimum entropy inverse convolutional adjustment method, which can extract the frequency

features of the acoustic emission signal of the bearings more accurately. Besides the aforementioned extraction techniques, Mean Influence Value (MIV) has garnered significant interest for its intuitive and efficient characteristics. In contrast to unsupervised dimensionality reduction techniques like Principal Component Analysis (PCA), MIV effectively preserves physically significant attributes directly associated with fault categories [15]. In contrast to approaches reliant on information entropy or correlation coefficients, MIV emphasizes the dynamic interplay between features and model outputs, rendering it more appropriate for input optimization in nonlinear network models, such as BPNNs [16].

It is important to note that while deep learning models have attained significant success in fault identification in recent years, their training necessitates a substantial quantity of labeled samples, and the model architecture is intricate, difficult to interpret, and resource-intensive [17]. In elevator bearing diagnosis, the limited training samples, high demand for real-time equipment response, and the simplicity, stable convergence, and interpretability of the BPNN model render it a more pragmatic option.

Therefore, this work proposes an MHO-BPNet fault diagnosis model to address the intricate and nonlinear failure modes in elevator fault signals, aiming for enhanced accuracy and reliability in elevator bearing fault diagnosis. The MHO-BPNet approach combines the MIV [18] and the Hippopotamus Optimization Algorithm (HO) [19] with Back Propagation Neural Networks (BPNNs) [20], and the efficacy of the proposed MHO-BPNet elevator bearing defect detection model is validated by two experimental sets. The contribution of this paper is:

(1) MHO-BPNet diagnostic model is presented for elevator bearing fault diagnosis, which can effectively utilize MIV to reduce the original features, identify fault-sensitive features, and enhance the reliability and stability of the fault diagnosis system.

(2) HO is employed to globally adjust the initial weights and thresholds of the backpropagation neural network (BPNN), successfully preventing the model from converging to local optima by mimicking the behavior of the hippopotamus population, while simultaneously enhancing the emphasis on critical local features.

(3) The efficacy of the proposed MHO-BPNet-based bearing fault diagnosis model is substantiated in the paper through analysis of two bearing datasets.

## II. Basic Research

### *II. A. Backpropagation neural networks (BPNNs)*

The BPNN is a multilayer feed-forward network with three layers, as illustrated in Figure 1. The layers are interconnected by weights, which directly influence the signal strength conveyed across the network [21].

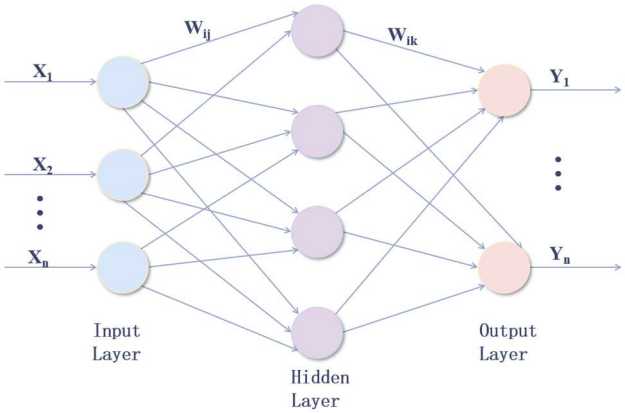


Figure 1: Topology of backpropagation neural network

The operation of the backpropagation neural network method can be systematically categorized into five stages [22]:

Stage 1: Forward propagation: data is introduced into the network via the input layer and sequentially processed by neurons in each layer, culminating in predictions produced by the output layer. The particular expression is denoted as equation (1):

$$A = f\left(\sum_{i=1}^{n} w_{ji} x_i + b_j\right) \tag{1}$$

where, $A$ indicates output result, $w_{ji}$ denotes weights form input layer to hidden layer, $x_i$ represents input value, $b_j$ is the bias of the $j$ neuron of the hidden layer.

Stage 2: Compute Error: the discrepancy is derived between the expected output and the target output [23].

Stage 3: Backpropagation: the error is transmitted from the output layer to the network, and the weights of each link are adjusted to minimize the error. This mistake is often assessed using the mean squared error (MSE) loss function.

$$MSE = \frac{\sum_{i=1}^{n}\left(y_i - y_i'\right)^2}{n} \tag{2}$$

where, $n$ represent sample values, $y_i$, $y_i'$ represent true and predicted values, $\left(y_i - y_i'\right)^2$ is the square of the difference between the $y_i$ and the $y_i'$.

Stage 4: Weight Update: The weights in the network are adjusted via alternative optimization algorithms, guided by the gradient of the error [24].

Stage 5: Iterative Process: The aforementioned procedure is reiterated until the network's output approximates the target output enough or a predetermined number of iterations is attained.

### *II. B.HO algorithm*

Mohammad Hussein Amiri et al. proposed the HO algorithm in 2024. The flowchart of the HO algorithm is shown in Figure 2.

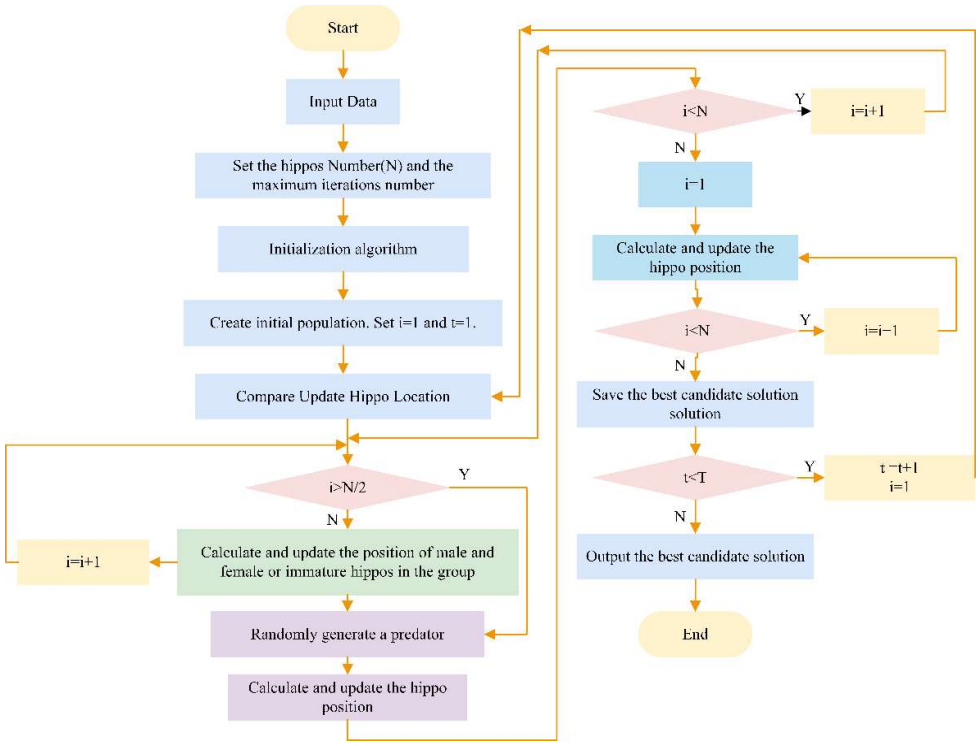


Figure 2: Flowchart of HO algorithm

#### II. B. 1) Initialization phase

Assuming that there are $n$ hippos and the $i$ hippo is at position $x_i$ in the space, the initialization can be expressed as

$$x_i : x_{i,j} = lb_j + r \cdot \left(ub_j - lb_j\right), i = 1,2,\ldots,N, j = 1,2,\ldots,m \tag{3}$$

where, $r$ indicates a random value in the range [0,1]. $ub_j$ and $lb_j$ indicates the lower and upper bounds of the $j$ variable. And $N$ indicates the number of hippos, $m$ indicates the number of variables.

**II. B. 2) Exploration phase**

During this phase, the algorithm emulates a hippopotamus adjusting its location in a river or pond, representing the global exploration phase of the method. The objective is to decentralize the search agents throughout the whole search space to enhance the likelihood of identifying the global best solution. Using the male hippopotamus as a case study, the formula can be articulated as:

$$X_i^{Mhippo} : X_{ij}^{Mhippo} = X_{ij} + y_1 \cdot \left( Dhippo - I_{1X_{ij}} \right) \tag{4}$$

where, $X_i^{Mhippo}$ indicates the new location of the male hippopotamus, $Dhippo$ indicates the position of the dominant hippo, $y_1$ indicates a random value, $X_{ij}$ indicates the current location of the hippopotamus. $I_1$ and $I_2$ indicates an integer of [1,2].

For juvenile or female hippopotamuses, the positional update equation is:

$$X_{i,j}^{FBhippo} = \begin{cases} X_{i,j} + h_1 \times \left( Dhippo - I_2 \times P_{MGi} \right), T > 0.6 \\ X_{i,j} + h_2 \times \left( I_2 \times P_{MGi} - Dhippo \right), T \le 0.6 \end{cases} \tag{5}$$

where, $X_{i,j}^{FBhippo}$ indicates the best position for a young hippopotamus or female hippopotamus, $P_{MGi}$ denotes the average position of a randomly selected hippopotamus, $h_1$ and $h_2$ is a randomly selected value, $I_2$ is a random integer, $T$ is the probability of deviation for immature hippos and their mothers.

**II. B. 3) Defense phase**

During this phase, the algorithm emulates the defensive behavior of the hippopotamus in response to predators, representing a balance between local search and exploration within the algorithm. The objective is to improve the algorithm's search within the vicinity of the existing best answer while continuing to explore new areas.

$$\vec{D} = \left| predator_j - x_{i,j} \right| \tag{6}$$

The above formula represents the distance from the $i$ hippo to the predator. As the predator approaches the hippo, the hippo moves toward the predator, forcing the predator to back away, $F_{predator}$ is larger the farther away the predator is from the hippopotamus. This can be expressed by the following equation:

$$X_i^{Mhippo} : X_{ij}^{Mhippo} = \begin{cases} \overrightarrow{RL} \oplus predator + \dfrac{f}{c - d \times \cos\left(2\pi g\right)} \cdot \dfrac{1}{\vec{D}}, F_{predator} < F_i \\ \overrightarrow{RL} \oplus predator + \dfrac{f}{c - d \times \cos\left(2\pi g\right)} \cdot \dfrac{1}{2\vec{D} + \vec{r}}, F_{predator} \ge F_i \end{cases} \tag{7}$$

where, $X_i^{Mhippo} : X_{ij}^{Mhippo}$ denotes the position of the hippopotamus facing the predator, $\overrightarrow{RL}$ denotes a random vector with Lévy distribution, $\vec{r}$ is a random vector. $c, d, f, g$ is a random variable used to model uncertainty in the location of the predator, $\vec{D}$ is the distance from the hippo to the predator.

If a hippopotamus is hunted, another will replace it in the herd, or the hunter will evade capture, allowing the hippopotamus to return to the herd, as illustrated by the following formula:

$$x_i = \begin{cases} x_i^{HippoR}, & F_i^{HippoR} < F_i \\ x_i, & F_i^{HippoR} \ge F_i \end{cases} \tag{8}$$

**II. B. 4) Escape phase**

This step involves the algorithm mimicking a hippopotamus evading a predator, representing the fine-tuning and exploitation stage of the program. The objective is to enhance the algorithm's search efficiency in the local vicinity to swiftly converge on the ideal answer. The formula presented below:

$$X_i^{Mhippo} : X_{ij}^{Mhippo} = X_{ij} + r_{10} \cdot lb_{local} + s \cdot \left( ub_{local} - lb_{local} \right) \tag{9}$$

where, $X_i^{Mhippo} : X_{ij}^{Mhippo}$ denotes the location of the hippopotamus escaping the predator, $r_{10}$ is a random value, and $lb_{local}$ and $ub_{local}$ denotes the lower and upper bounds of the local search space, and $s$ denotes chosen from the following equation:

$$s = \begin{cases} 2 \times \vec{r}_{11} - 1 \\ r_{12} \\ r_{13} \end{cases} \tag{10}$$

where, $\vec{r}_{11}$ and $r_{13}$ denotes a random value of [0,1]. Furthermore, $r_{12}$ denotes a normally distributed random value.

### *II. C.Mean Impact Value (MIV)*

In the real implementation of neural network models, it is essential to filter input variables to eliminate superfluous elements that prolong training time and diminish model accuracy. The prevalent methodologies employed include PAC, Factor Analysis (FA), and MIV, with the performance disparity described in Table 1.

The sign of MIV denotes the direction of its effect on the output variable, while the magnitude of its absolute value reflects the extent of that influence. The specific steps are [25]:

Step 1: In the neural network architecture, the training samples are augmented and reduced by 10% correspondingly to create two new training datasets.

Step 2: Employ the created neural network model to simulate the two modified samples, acquire two simulation outcomes, and subtract these results to determine the extent of the change in impact degree.

Step 3: The IV is averaged to derive the MIV of the network output, calculated according to equation (11): $n$ for sample values, $y_{up}(i)$ and $y_{down}(i)$ are the outputs of the neural network in the $i$ sample when the input variable is increased by 10% and decreased by 10%.

$$MIV = \frac{1}{n} \sum_{i=1}^{n} \left( y_{up}(i) - y_{down}(i) \right) \tag{11}$$

Step 4: Reiterate the preceding processes to ascertain the MIV of each feature indicator and select the corresponding feature indication based on the magnitude of the MIV.

Table 1: Difference table of dimensionality reduction methods

| | Influencing factors | Linear/non-linear | Accuracy |
|---|---|---|---|
| PCA | First Principal | Linear | Good |
| FA | Specified Factor | Linear | Average |
| MIV | Almost no effect | Nonlinear | Better |

### *II. D.Fault diagnosis model*

This study utilizes the MIV method with HO to optimize BPNN. The flowchart of the algorithm for the established MHO-BPNet model is presented in Figure 3. The steps are as follows:

Step 1: Input bearing data and standardize the data.

Step 2: Organize the feature indicators utilizing the MIV method.

Step 3: The organized feature indicators are integrated into the HO algorithm utilizing a backpropagation neural network.

Step 4: Initialize the backpropagation neural network.

Step 5: Establish the fitness function via a backpropagation neural network and include it into the HO algorithm.

Step 6: Assess the present racial fitness and revise and save it utilizing the initial position of the hippopotamus and the three behaviors of the HO algorithm.

Step 7: Ascertain if the algorithm meets the stipulated conditions. Upon fulfillment of the prerequisites, revert to step 6 to revise the three defensive actions of the HO algorithm. If the requirement is unmet, proceed to step 8 to present the current optimal solution.

Step 8: Acquire the optimal solution of HO and train the backpropagation neural network for fault diagnosis.

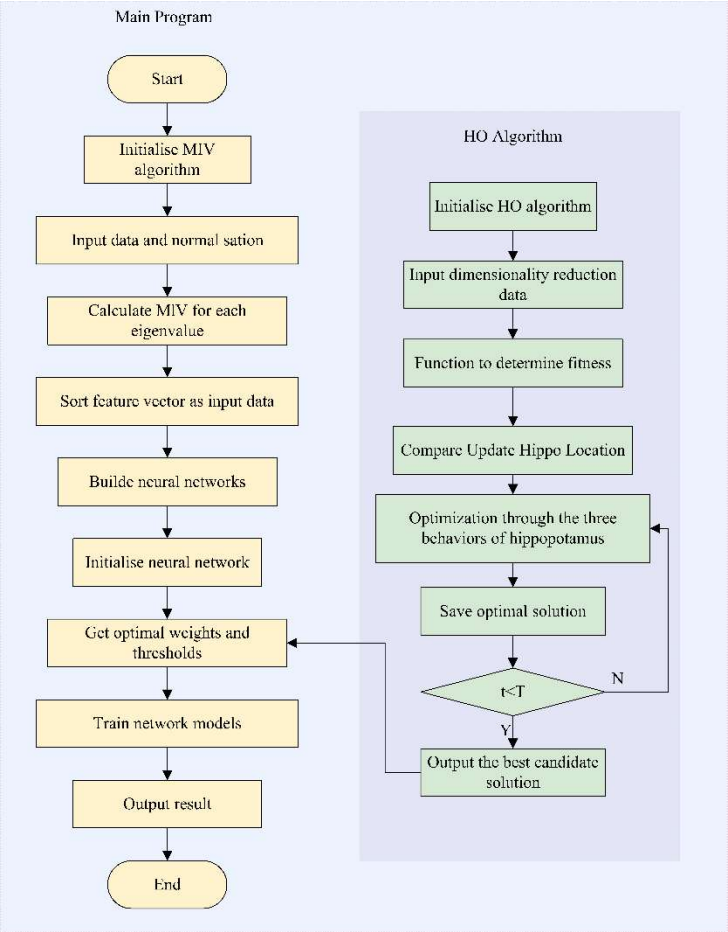


Figure 3: Flowchart of MHO-BPNet modeling algorithm

The further parameters are as follows: the number of iteration rounds is 1000, the learning rate is 0.001, the training accuracy is 10-6, and the number of failures is 6. The selection of seven hidden layers is warranted when the input and output layers consist of four and ten nodes, respectively, as evidenced by Table 2, because to the varying differentials associated with differing numbers of hidden layers. Tansig, purelin, and trainlm are activation functions for the hidden layer, output layer, and training, respectively.

Table 2: Number of nodes in the hidden layer

| Number of hidden layer nodes | Training Set MSE | Number of hidden layer nodes | Training Set MSE |
|---|---|---|---|
| 4 | 0.048585 | 7 | 0.017678 |
| 5 | 0.039342 | 8 | 0.019172 |
| 6 | 0.030574 | —— | ———— |

## III. Experimental analyses

This subsection will conduct experimental validation utilizing bearing data from Case Western Reserve University (CWRU) [26] and Shandong University of Science and Technology (SDUST) [27].

In order to prove the effectiveness of MHO-BPNet, this paper will and SVM, BPNN optimized with MIV using Particle Swarm Optimization (PSO) algorithm, and a new algorithm combining MIV using Love Evolutionary Algorithm (LEA). That is, the three algorithms SVM, MIV-PSO-BP and MIV-LEA-BP are compared with the MHO-BPNet algorithm proposed in this paper in terms of error, volatility and accuracy. All the above four methods are trained and classified using the features extracted in this paper.

The initialization of the neural network, including the weights and thresholds during training, may influence the final output outcomes. Therefore, this paper trained each model 20 times to more precisely capture the variations

in prediction performance among different models, evaluating them using mean square error (MSE), mean absolute error (MAE), and cross-entropy loss parameters, calculated according to the formulas provided below:

$$MSE = \frac{\sum_{i=1}^{n}\left(y_i - y_i'\right)^2}{n} \tag{12a}$$

$$MAE = \frac{\sum_{i=1}^{n}\left|y_i - y_i'\right|}{n} \tag{12b}$$

$$LOSS = \sum_{i=1}^{n} y_i \log\left(y_i'\right) \tag{12c}$$

where, $n$ for sample values, $y_i$, $y_i'$ for true and predicted values, $\left(y_i - y_i'\right)$ and $\left|y_i - y_i'\right|$ are the difference and absolute value between the $y_i$ and the $y_i'$.

This paper extracts nine feature indicators from the bearing failure dataset, as presented in Table 3 and employs the MIV as a tool to investigate the interrelationships among these variables. The MIV algorithm ranks the significance of the distinctive indications from high to low, with the results illustrated in Figure 4. Combined with Table 3 illustrates that the feature indicators exerting the most significant influence on diagnostic outcomes are the effective value and impulse factor, followed by the margin factor. The effective value directly indicates the operational condition of the bearing, whereas the impulse factor and margin factor effectively demonstrate bearing failure under shock vibration and facilitate the assessment of the bearing's residual life and failure severity. The mean value, pulse factor, margin factor, and peak value in the characteristic indices mostly represent a mathematical trend and do not correlate with the bearings, thus exerting minimal impact on the diagnostic outcomes.

Table 3: Indicators of Bearing Failure Characteristics

| Number | Feature | Number | Feature |
|---|---|---|---|
| 1 | Mean | 6 | Peak Factor |
| 2 | Variance | 7 | Pulse Factor |
| 3 | Peak | 8 | Shape Factor |
| 4 | Kurtosis | 9 | Margin Factor |
| 5 | Effective Value | — | ———— |

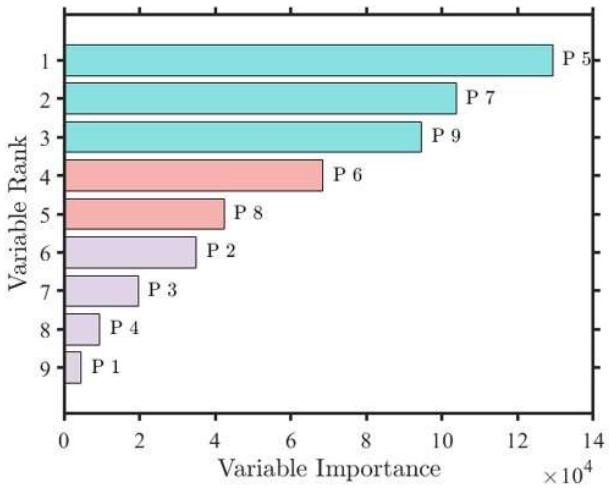


Figure 4: Significance of Characterization Indicators

### *III. A. CWRU Data Analysis*

The CWRU bearing dataset is commonly utilized for research on bearing defect identification and diagnosis. CWRU is publically accessible and comprises data on the operational conditions of four distinct bearing types: inner-ring faults, outer-ring faults, rolling-body faults, and normal status. The data collecting is illustrated in Figure 5. The test stand comprises a motor, a torque transducer, a power tester, and control electronics (not depicted). The bearing under examination supports the motor, and the test employs EDM to create a single point of failure in the test bearing.

The driving end bearing is SKF6205 for fault testing with diameters of 7, 14, and 21 mm, with collection frequencies of 12 kHz and 48 kHz. The fan end bearing is an NTN equivalent bearing for 28 mil and 40 mil fault testing, with a collection frequency of 12 kHz. In the experiment, when the collection frequency at the driving end is 12 kHz and 48 kHz, the data from the inner ring and the rolling element may be immediately measured, recorded, and saved in MATLAB format.

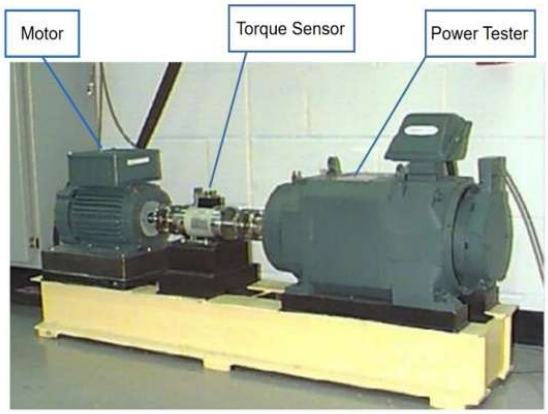


Figure 5: CWRU Bearing Experimental Setup

#### III. A. 1) t-SNE visualization

The article employs the t-SNE [28] approach to show the original data and the four optimization algorithms, thereby clearer of the MHO-BPNet algorithm.

Figure 6 illustrates the result of t-SNE visualization. t-SNE [28] is employed to visualize high-dimensional datasets. Its objective is to preserve the local structure of high-dimensional data, illustrating the relative distances and similarities among the data, rather than explicitly indicating the model's predictive accuracy. The original data figure (a) illustrates that the untrained segment is in a chaotic and disorganized condition, with several flaws conflated, complicating their classification. Figure 6 (d) illustrates the t-SNE plot subsequent to the application of the SVM algorithm. In comparison to the original data, the chaotic and disordered data has been categorized, with the most chaotic conditions persisting in the lower right quadrant; nonetheless, a degree of confusion remains when juxtaposed with the other three plots.

Figure 6 (b) illustrates that the MHO-BPNet algorithmic model proposed in this paper effectively delineates fault classifications, exhibiting little misclassification across analogous fault data compared to prior models.

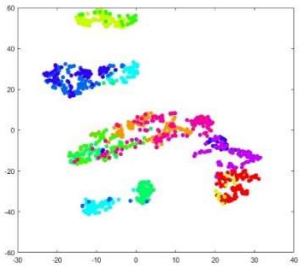

a) Raw data

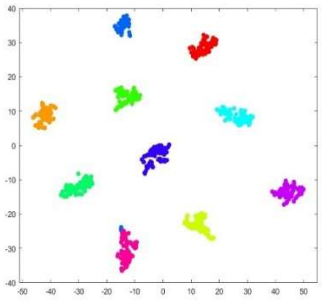

b) MHO-BPNet

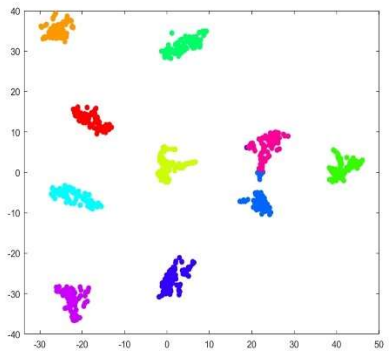

c) MIV-LEA-BP

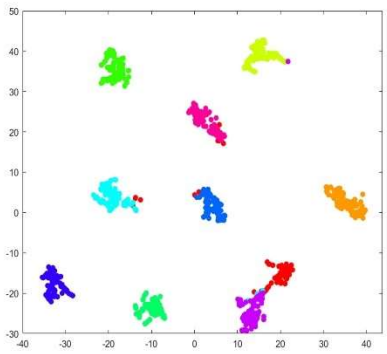

d) SVM

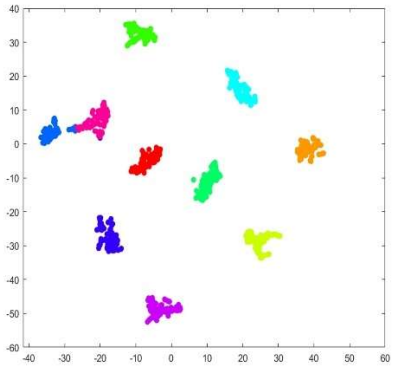

e) MIV-PSO-BP

Figure 6: t-SNE visualization

**III. A. 2) Accuracy analysis**

This research employs a confusion matrix to present the experimental results more plainly; Figure 7 illustrates the confusion matrix depicting the accuracy of each algorithm.

The color gradients in the confusion matrix indicate classification accuracy, while the diagonal lines signify correctness. The classification mistakes of the models optimized by LEA manifest in three, five, seven, and nine categories, with the MIV-PSO-BP algorithm model exhibiting the maximum number of misclassified categories; nonetheless, its accuracy is inferior to that of the model described in this article. MHO-BPNet has the fewest classification mistakes and the best accuracy. Equation (13) delineates the formula for the correctness of the confusion matrix, where $TP$ is predicted and actual values are positive, $TN$ is negative forecast and actual, $TP$ and $FN$ is predictions are the opposite of reality. Validation calculations following equation (13) indicate that the classification accuracy of the proposed MHO-BPNet algorithm reaches 97.8%, while the MIV-LEA-BP model achieves 94.25%, the SVM attains 96.2%, and the MIV-PSO-BP records 95.3%. This demonstrates that the MHO-BPNet algorithm outperforms other optimization algorithm models.

$$Accuracy = \frac{TP + TN}{TP + TN + FP + FN} \tag{13}$$

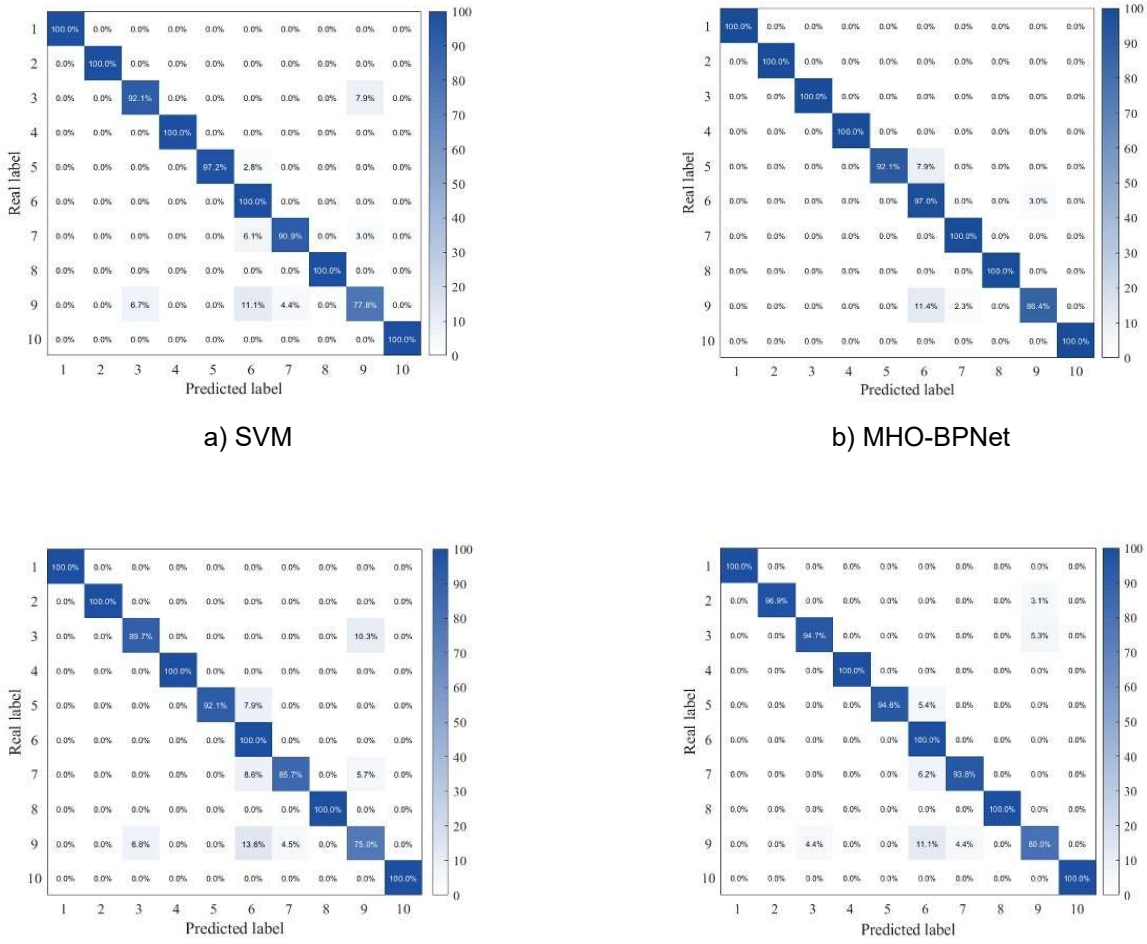


a) SVM

b) MHO-BPNet

c) MIV-LEA-BP

d) MIV-PSO-BP

Figure 7: Accuracy analysis

**III. A. 3) Error analysis**

To objectively assess the merits and drawbacks of the aforementioned four techniques, 20 iterations of each algorithm were conducted, utilizing MAE and MSE as evaluative criteria for comparison. A minimal difference between the two is preferable. It is important to note that SVM cannot compute the MAE and MSE, so they are not addressed in the subsequent analysis. Tables 4 and 5 present the comparative statistics for MAE and MSE. The table indicates that the MHO-BPNet method has strong performance in both MAE and MSE metrics. The average value of MHO-BPNet on the MAE indicator is 0.032929, the lowest among all algorithms, signifying the minimal prediction error; on the MSE indicator, the average value is 0.010570, also the lowest, further substantiating its preeminence in error management. The unequivocally illustrate the advantages of the MHO-BPNet method regarding accuracy and stability.

Table 4: Comparison of MAE of algorithms (CWUR)

| | Best Value | Worst Value | Average Value |
|---|---|---|---|
| MHO-BPNet | 0.033198 | 0.032708 | 0.032929 |
| MIV-LEA-BP | 0.040012 | 0.039854 | 0.039972 |
| MIV-PSO-BP | 0.042641 | 0.042169 | 0.042547 |

Table 5: Comparison of MSE of algorithms (CWUR)

| | Best Value | Worst Value | Average Value |
|---|---|---|---|
| MHO-BPNet | 0.010807 | 0.010377 | 0.010570 |
| MIV-LEA-BP | 0.015375 | 0.014287 | 0.014559 |
| MIV-PSO-BP | 0.014502 | 0.010801 | 0.013762 |

**III. A. 4) Volatility analysis**

The algorithms' volatility is typically employed to evaluate their stability and predictability; however, considering the variations in outcomes across multiple diagnoses, this study conducted 20 iterations, with the volatility results illustrated in Figure 8. Figure 8 illustrates the iterations on the X-axis, while the Y-axis represents the standard deviation. A higher value on the vertical axis indicates poorer stability of the algorithm. The figure demonstrates that, due to the randomness of the initialization parameters, all three algorithms exhibit significant fluctuations, with the LEA optimization algorithm displaying the most pronounced variability, evidenced by a standard deviation of 0.00043892. In contrast, the MHO-BPNet algorithm shows the least fluctuation, with a standard deviation of 0.00030185, while the PSO optimization algorithm falls in between, recording a standard deviation of 0.00035935. This shows that the MHO-BPNet algorithm performs best.

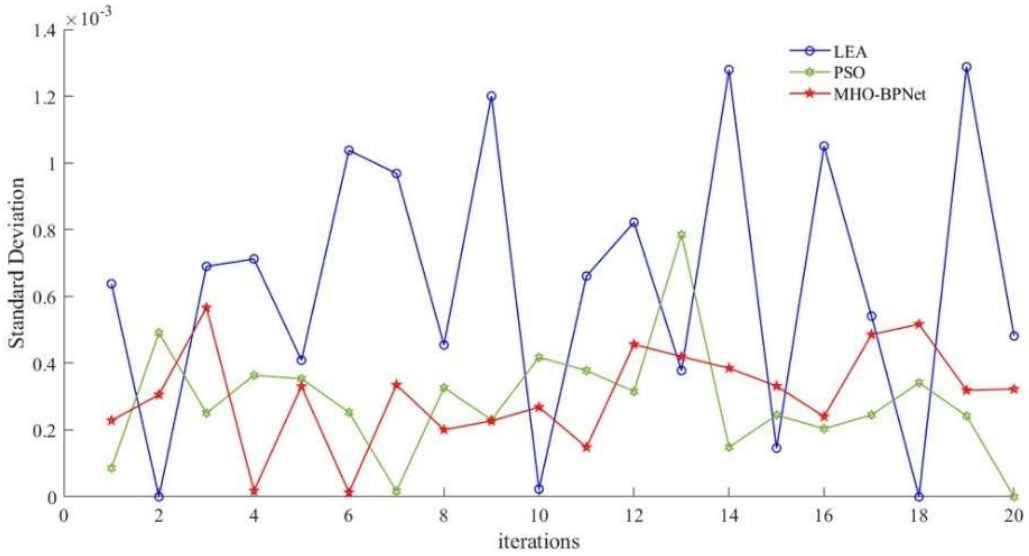


Figure 8: Volatility results

***III. B. SDUST Data Analysis***

To further substantiate the viability of the algorithm presented in this paper, the bearing dataset from SDUST is utilized once more for validation. The test stand comprises an AC motor, a bearing under examination, a gearbox, and a magnetic powder brake for load regulation, among other components. It is designed to conduct fault diagnosis tests on various types of rolling bearings and gears under diverse operational conditions. The specific test component is the 6205 bearing, as illustrated in Fig 9. The LMS company's laboratory vibration and noise testing system is employed to gather vibration signals during the collection. The test is conducted in steady state testing mode, with a sampling interval of 40 seconds and a sampling frequency of 25.6 kHz. The characteristic indices are identical to those chosen by CWUR, including mean value, variance, peak factor, and nine additional indices.

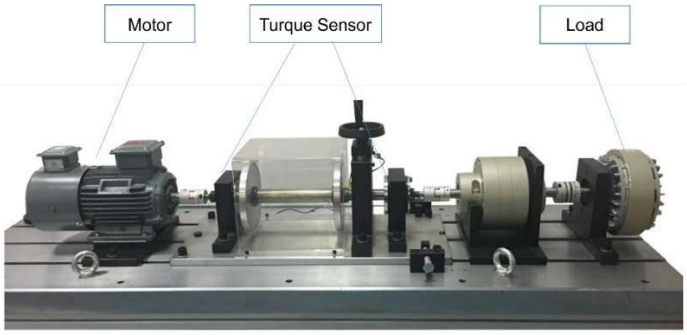


Figure 9: Bearing test bench of STUSD

**III. B. 1) Accuracy analysis**

Figure 10 displays the confusion matrix for each algorithmic model utilizing the bearing data from SDUST.

The figure indicates that MHO-BPNet exhibits less than 90% accuracy alone in the first and eighth categories, whereas all other optimization algorithm models demonstrate mistakes in more than two categories, with SVM being the most frequently misclassified category. The computation of equation (13) indicates that the proposed technique achieves an accuracy of 96.9%, while MIV-PSO-BP attains 84.88%, MIV-LEA-BP reaches 90.74%, and SVM records an accuracy of merely 92.59%. The strategy presented in this paper enhances accuracy by around 2% to 10% relative to existing optimization strategies.

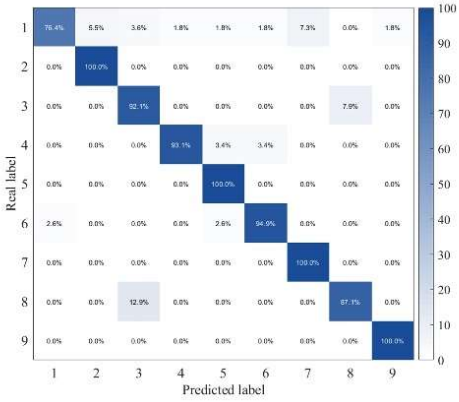


a) SVM

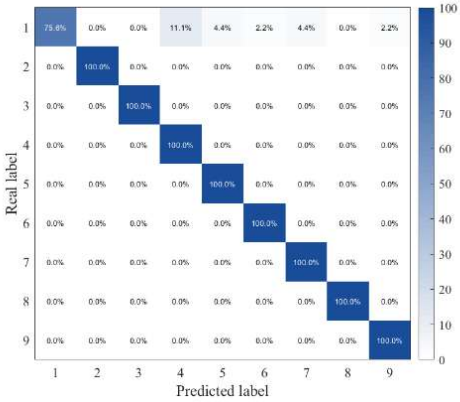


b) MHO-BPNet

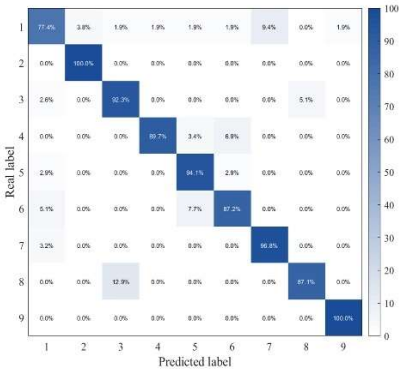


c) MIV-LEA-BP

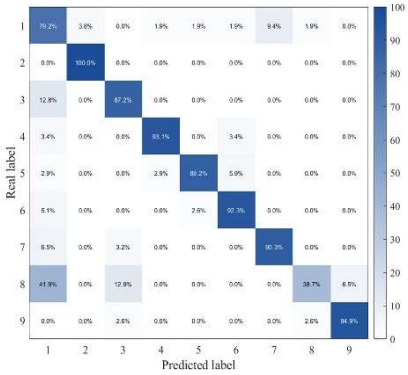


d) MIV-PSO-BP

Figure 10: Accuracy analysis

**III. B. 2) Error analysis**

This dataset similarly employs the same number of iterations as CWRU and utilizes MSE and MAE as assessment metrics. Table 6 and Table 7 present the comparative statistics of MAE and MSE for the bearing data from SDUST, indicating that the MIV-PSO-BP algorithm model excels in MAE and MSE; however, it does not surpass the accuracy of the approach proposed in this paper. Secondly, the MHO-BPNet algorithm model is merely 0.655% inferior in comparison. Despite the MHO-BPNet not achieving optimal performance on this dataset, it exhibits the highest accuracy rate, as demonstrated above, indicating that the approach suggested in this research possesses remarkable generalization capability and generalizability.

Table 6: Comparison of MAE of algorithms (SDUST)

| | Best Value | Worst Value | Average Value |
|---|---|---|---|
| MHO-BPNet | 0.105128 | 0.101245 | 0.104546 |
| MIV-LEA-BP | 0.121056 | 0.117256 | 0.119346 |
| MIV-PSO-BP | 0.104444 | 0.104444 | 0.104444 |

Table 7: Comparison of MSE of algorithms (SDUST)

| | Best Value | Worst Value | Average Value |
|---|---|---|---|
| MHO-BPNet | 0.075103 | 0.069643 | 0.074284 |
| MIV-LEA-BP | 0.102848 | 0.091685 | 0.097825 |
| MIV-PSO-BP | 0.071814 | 0.071814 | 0.071814 |

**III. B. 3) Volatility analysis**

To facilitate comparison and validation, the volatility iterations for this data set are selected 20 times; Figure 11 illustrates the volatility of the bearing data set. The figure illustrates that the blue line represents the algorithmic model optimized by LEA, exhibiting the greatest fluctuation range, with a volatility of 0.0020885. In contrast, the algorithmic model optimized by MHO-BPNet demonstrates a volatility of 0.00085231, while the model optimized by PSO shows a volatility of 0.00091474. The comparison of these two datasets indicates that the MHO-BPNet model has more stability.

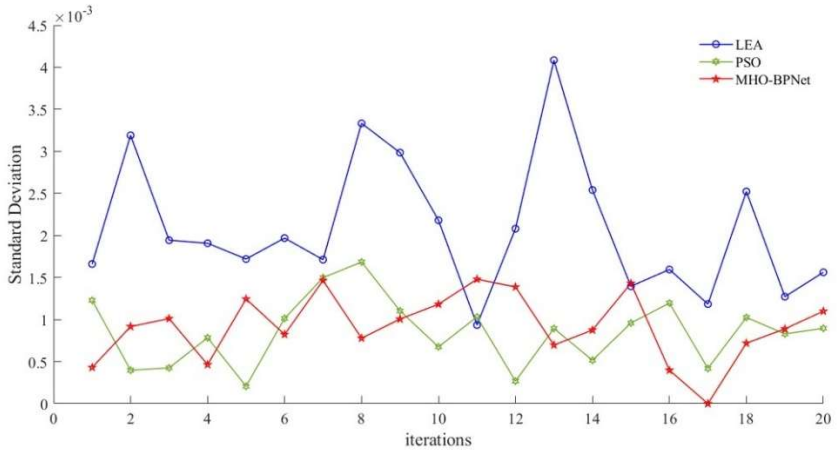


Figure 11: Volatility of the SDUST bearing dataset

***III. C. Ablation experiment***

This paper presents two ablation experiments to validate the advantages of the proposed MHO-BPNet algorithm. The neural network, following MIV dimensionality reduction, is utilized just in Experiment A, while Experiment B employs a singular BPNN. Both experiments are conducted on the CWRU dataset to ensure the integrity of the experiments.

Figure 12 illustrates the confusion matrix for Experiment A and Experiment B. The confusion matrix and Equation (13) indicate that the accuracy of Experiment B, utilizing only BPNNs, is 92.02%. Following MIV dimensionality reduction, the accuracy increases to 93.48%, reflecting an enhancement of 1.46%. This enhancement demonstrates

the essentiality of the MIV method. Likewise, the imperative of the HO algorithm is evident in subsection 3.1.2, where it attains superior accuracy relative to PSO, LEA, and other optimization techniques.

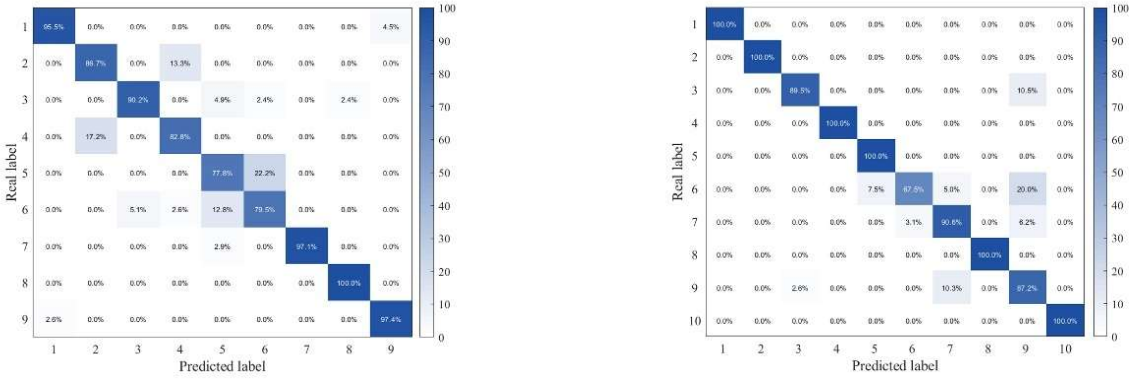


a) BP b) MIV-BP

Figure 12: Experiment A and Experiment B confusion matrices

### *III. D. Discussions*

This study demonstrated that the proposed hybrid MHO-BPNet model for elevator bearing fault diagnosis attained accuracies of 97.8% and 96.9% on two distinct datasets, significantly surpassing the performance of other algorithms: 94.25% and 90.74% for LEA; 95.3% and 84.88% for PSO; and 96.2% and 92.59% for SVM. This outcome unequivocally illustrates the model's overall superiority and capacity for generalization. A comprehensive analysis of model performance enhancement arises from the effective integration of essential components: firstly, the MIV feature dimensionality reduction markedly enhances model efficiency and generalization by identifying and discarding redundant and noisy features. The ablation experiment substantiates that the accuracy of the original BPNN can be elevated to 93.48% solely through the application of MIV, underscoring the critical importance of MIV preprocessing. Secondly, the HO algorithm significantly enhances the optimization of the initial weights and thresholds of the BPNN. In ablation experiments, the accuracy rate after implementing HO shows an improvement of 4.32% and 3.42% on dataset one and dataset two, respectively, and surpasses optimizers such as PSO and LEA. This effectively addresses the inherent limitations of the BPNN, which is susceptible to local optima and sensitive to initial parameters. This study presents a dependable intelligent diagnostic framework for the safe operation and maintenance of elevators, enabling the identification of faults in elevator bearings, hence minimizing unplanned outages and ensuring passenger safety.

## IV. Conclusions

This research proposes an MHO-BPNet methodology for diagnosing faults in elevator bearings to enhance accuracy and generalizability. Moreover, numerous comparative experiments are performed. The experiments validate the accuracy and practicality of the fault diagnosis method. The principal conclusions are as follows:

(1) The MIV approach diminishes the impact of redundant features on the neural network, resulting in enhanced input data and improved capabilities for subsequent problem diagnostics.

(2) The optimization of BPNNs through the incorporation of the HO algorithm significantly enhances both convergence speed and optimality performance.

(3) The MHO-BPNet model for elevator fault diagnosis accurately identifies the condition of elevator bearings, achieving a fault diagnosis accuracy exceeding 96.5% in both datasets.

The technology presented in this paper has yielded favorable outcomes in elevator bearings. Nonetheless, it is imperative to address enhanced concerns in the future, including real-time monitoring and diagnosis of the elevator, to ensure prolonged operation and greater reliability.

## Acknowledgements

This research was funded by The Science and Technology Project of Hebei Education Department. (Grant No. CXZX2025039)

## Data availability

The datasets generated during and/or analyzed during the current study are available from the corresponding author on reasonable request.

## Author contributions

Qiang Li's contributor role are supervision, conceptualization and methodology. Rundong Zhou's contributor role is methodology, explore, validation, writing-original draft preparation and writing-review and editing. Xinyu Zhai's contributor role are data curation and software. Qing Lv's contributor role are supervision and resources.

## Conflict of interest

The authors declare that they have no conflict of interest.

## References


[1] Zhaoming Luo, Gang Xu, Wenjun Ouyang, Mingze Ni, Jiazong Wu, "Leveraging Prior Knowledge and Synthetic Data for Elevator Anomaly Object Segmentation," Electronics, 2025, 14 (10): https://doi.org/10.3390/electronics14101970

[2] Haokun Wu, Qiwei Tang, Li Yin, Wang Zhang, "Fault diagnosis of elevator systems based on multidomain feature extraction and SHAP feature selection," Building Services Engineering Research & Technology, 2025, 46 (3): http://dx.doi.org/10.1177/01436244241309205

[3] Prahlow Joseph A, Ashraf Zuhha, Plaza Natalie, Rogers Christopher, Ferreira Pamela, Fowler David R, Blessing Melissa M, Wolf Dwayne A, Graham Michael A, Sandberg Kelly, Brown Theodore T, Lantz Patrick E, "Elevator-Related Deaths," Journal of forensic sciences, 2020, 65 (3): https://doi.org/10.1111/1556-4029.14235

[4] Teng Wang, Zhi Chao Ong, Shin Yee Khoo, Pei Yi Siow, Jinlai Zhang, Tao Wang, "SeqInfo-SAWGAN-GP: Adaptive feature extraction from vibration time data under variable operating conditions for imbalanced bearing fault diagnosis," Measurement, 2025, 243 https://doi.org/10.1016/j.measurement.2024.116344

[5] Jiali Wang, Chengjiang Zhou, Zhiwei Zhang, Na Meng, Guirong Du, Xuepeng Jin, Cailing Zhang, "A fault diagnosis method using decomposition denoising improved multiscale weighted permutation entropy and one-versus-one least squares twin SVM," Measurement, 2025, 255 https://doi.org/10.1016/j.measurement.2025.118012

[6] Mao Xiaodong, "Cross domain fault diagnosis method based on MLP-mixer network," Journal of Measurements in Engineering, 2023, 11 (4): https://doi.org/10.21595/jme.2023.23460

[7] Sinitsin V, Ibryaeva O, Sakovskaya V, Eremeeva V, "Intelligent bearing fault diagnosis method combining mixed input and hybrid CNN-MLP model," Mechanical Systems and Signal Processing, 2022, 180 https://doi.org/10.1016/j.ymssp.2022.109454

[8] Yanqiu Wu, Juying Dai, Xiaoqiang Yang, Faming Shao, Jiancheng Gong, Peng Zhang, Shaodong Liu, "The Fault Diagnosis of Rolling Bearings Based on FFT-SE-TCN-SVM," Actuators, 2025, 14 (3): https://doi.org/10.3390/act14030152

[9] Kumar Rajeev, Anand R. S, "Bearing fault diagnosis using multiple feature selection algorithms with SVM," Progress in Artificial Intelligence, 2024, 13 (2): https://doi.org/10.1007/s13748-024-00324-1

[10] Yang C, Jia M, "Hierarchical multiscale permutation entropy-based feature extraction and fuzzy support tensor machine with pinball loss for bearing fault identification," Mechanical Systems and Signal Processing, 2021, 149 https://doi.org/10.1016/j.ymssp.2020.107182

[11] Wang Haiming, Li Qiang, Yang Shaopu, Liu Yongqiang, "Fault Recognition of Rolling Bearings Based on Parameter Optimized Multi-Scale Permutation Entropy and Gath-Geva," Entropy, 2021, 23 (8): https://doi.org/10.3390/e23081040

[12] Li Zhe, Li Longlong, Chen Runlin, Zhang Yanchao, Cui Yahui, Wu Ningqiang, "A novel scheme based on modified hierarchical time-shift multi-scale amplitude-aware permutation entropy for rolling bearing condition assessment and fault recognition," Measurement, 2024, 224 https://doi.org/10.1016/j.measurement.2023.113907

[13] Guo Huijuan, "Fault diagnosis of rolling bearing under complex working conditions based on time-frequency joint feature extraction-deep learning," Journal of Vibroengineering, 2024, 26 (7): https://doi.org/10.21595/jve.2024.24238

[14] Yun Li, Yang Yu, Ping Yang, Fanzi Pu, Yunpeng Ben, "Acoustic Emission Signal Feature Extraction for Bearing Faults Using ACF and GMOMEDA," Journal of Nondestructive Evaluation, 2024, 43 (4): https://doi.org/10.1007/s10921-024-01134-0

[15] Li Ning, He Fuxing, Ma Wentao, Wang Ruotong, Jiang Lin, Zhang Xiaoping, "The Identification of ECG Signals Using Wavelet Transform and WOA-PNN," Sensors (Basel, Switzerland), 2022, 22 (12): https://doi.org/10.3390/s22124343

[16] Chen Songgui, Chen Hanbao, Peng Cheng, Wang Yina, Hu Yuanye, "Analysis of Factors Influencing Wave Overtopping Discharge from Breakwater Based on an MIV-BP Estimation Model," Water, 2022, 14 (19): https://doi.org/10.3390/w14192967

[17] Lipton, Z. C, "The Mythos of Model Interpretability: In machine learning, the concept of interpretability is both important and slippery," ACM Queue, 2018, 16(3), 31–57. https://doi.org/10.1145/3236386.3241340

[18] Chun-Yao Lee, Yi-Xing Shen, "Optimal Feature Selection for Power-Quality Disturbances Classification," IEEE Transactions on Power Delivery, 2011, 26 (4): 10.1109/TPWRD.2011.2149547

[19] R. Amirulaminnur, M. Firdaus Isham, M. K. Harith, M. S. R. Saufi, W. A. A. Saad, M. D. A. Hasan, M. H. A. Talib, "Extreme Learning Machine Optimization based on Hippopotamus Optimization Algorithm for Gear Fault Diagnosis," Journal of Physics: Conference Series, 2025, 2933 (1): https://dx.doi.org/10.1088/1742-6596/2933/1/012019

[20] Wu Qiang, Wang Yu, Wang Yaoping, Wang Jian, Lan Lei, Deng Yeqiang, Wen Xishan, Luo Bing, Xiao Wei, "Ablation state assessment of SF6 circuit breaker contacts based on BP neural network and mean impact value," Energy Reports, 2022, 8 (S5): https://doi.org/10.1016/j.egyr.2022.02.237

[21] Rumelhart, D., Hinton, G. & Williams, R, "Learning representations by back-propagating errors," Nature 323, 533–536 (1986). https://doi.org/10.1038/323533a0

[22] Rui Jiao, Sai Li, Zhixia Ding, Le Yang, Guan Wang, "Fault diagnosis of rolling bearing based on BP neural network with fractional order gradient descent," Journal of Vibration and Control, 2024, 30 (9-10): http://dx.doi.org/10.1177/10775463231175267

[23] Intelligence And Neuroscience Computational, "Retracted: Intelligent Detection and Diagnosis of Power Failure Relying on BP Neural Network Algorithm," Computational intelligence and neuroscience, 2023, 2023 https://doi.org/10.1155/2023/9858071

[24] Zhiliang Z, Xiaofeng X, Lujia L, “A Novel GA—BP Neural Network for Wireless Diagnosis of Rolling Bearing,” Journal of Circuits, Systems and Computers, 2022, 31(10): https://doi.org/10.1142/S0218126622501730
[25] Lee ChunYao, Ou HongYi, “Induction Motor Multiclass Fault Diagnosis Based on Mean Impact Value and PSO-BPNN,” Symmetry, 2021, 13 (1): https://doi.org/10.3390/sym13010104
[26] Wade A. Smith, Robert B. Randall, “Rolling element bearing diagnostics using the Case Western Reserve University data: A benchmark study,” Mechanical Systems and Signal Processing, 2015, 64-65 https://doi.org/10.1016/j.ymssp.2015.04.021
[27] Wang Jinrui, Zhang Xuepeng, Zhang Zongzhen, Han Baokun, Jiang Xue, Bao Huaiqian, Jiang Xingxing, “Attention guided multi-wavelet adversarial network for cross domain fault diagnosis,” Knowledge-Based Systems, 2024, 284 https://doi.org/10.1016/j.knosys.2023.111285
[28] Laurens, Van Der Maaten, and G. Hinton , “Visualizing Data using t-SNE,” Journal of Machine Learning Research 9.2605(2008):2579-2605.
[29]